



# Lab on a Chip

## Compact wide-field femtoliter-chamber imaging system for high-speed and accurate digital bioanalysis

Journal:	<i>Lab on a Chip</i>
Manuscript ID	LC-ART-08-2022-000741.R1
Article Type:	Paper
Date Submitted by the Author:	11-Oct-2022
Complete List of Authors:	Iida, Tatsuya; RIKEN, Cluster for Pioneering Research Ando, Jun; RIKEN, Cluster for Pioneering Research Shinoda, Hajime; RIKEN, Cluster for Pioneering Research Makino, Asami; RIKEN, Cluster for Pioneering Research Yoshimura, Mami; RIKEN, Cluster for Pioneering Research Murai, Kazue; RIKEN, Cluster for Pioneering Research Mori, Makiko; RIKEN, Cluster for Pioneering Research Takeuchi, Hiroaki; Tokyo Medical and Dental University Noda, Takeshi; Kyoto University Nishimasu, Hiroshi; The University of Tokyo Watanabe, Rikiya; RIKEN, Cluster for Pioneering Research

SCHOLARONE™  
Manuscripts

## Compact wide-field femtoliter-chamber imaging system for high-speed and accurate digital bioanalysis†

Tatsuya Iida<sup>a,‡</sup>, Jun Ando<sup>a,‡</sup>, Hajime Shinoda<sup>a</sup>, Asami Makino<sup>a</sup>, Mami Yoshimura<sup>a</sup>, Kazue Murai<sup>a</sup>, Makiko Mori<sup>a</sup>, Hiroaki Takeuchi<sup>b</sup>, Takeshi Noda<sup>c</sup>, Hiroshi Nishimasu<sup>d,e</sup> and Rikiya Watanabe<sup>\*a</sup>

Received 00th January 20xx,  
Accepted 00th January 20xx

DOI: 10.1039/x0xx00000x

The femtoliter-chamber array is a bioanalytical platform that enables highly sensitive and quantitative analysis of biological reactions at the single-molecule level. This feature has been considered a key technology for “digital bioanalysis” in the biomedical field; however, its versatility is limited by the need for a large and expensive setup such as a fluorescence microscope, which requires a long time to acquire the entire image of a femtoliter-chamber array. To address these issues, we developed a compact and inexpensive wide-field imaging system (COWFISH) that can acquire fluorescence images with a large field of view (11.8 mm × 7.9 mm) and a high spatial resolution of ~ 3 μm, enabling high-speed analysis of sub-million femtoliter chambers in 20 s. Using COWFISH, we demonstrated a CRISPR-Cas13a-based digital detection of viral RNA of SARS-CoV-2 with an equivalent detection sensitivity (limit of detection: 480 aM) and a 10-fold reduction in total imaging time, as compared to confocal fluorescence microscopy. In addition, we demonstrated the feasibility of COWFISH to discriminate between SARS-CoV-2-positive and -negative clinical specimens with 95% accuracy, showing its application in COVID-19 diagnosis. Therefore, COWFISH can serve as a compact and inexpensive imaging system for high-speed and accurate digital bioanalysis, paving a way for various biomedical applications, such as diagnosis of viral infections.

### Introduction

Digital bioanalysis using femtoliter-chamber (fL-chamber) arrays is an emerging approach for detecting various biological reactions<sup>1, 2</sup>, including hydrolysis<sup>3</sup>, protein synthesis<sup>4</sup>, and membrane transport<sup>5, 6</sup>, with high sensitivity down to the single-molecule level, thereby facilitating biomedical applications such as diagnosis of cancer, Alzheimer’s disease, and viral infections<sup>7–11</sup>. In enzyme-based digital bioanalysis, the reaction solution is partitioned into fL-chamber arrays that are highly integrated on a chip, allowing most chambers to be loaded with 0 or 1 target molecule. Since the target molecule of enzyme-based digital bioanalysis is assumed to i) have its own enzymatic activity, ii) bind to an enzyme with an antibody, or iii) act as an activator of an enzyme, the enzymatic product derived from a single target molecule is accumulated and concentrated in the chamber over time. Owing to the femtoliter volume of chambers, the concentration of the enzymatic product increases drastically and rapidly; therefore, the presence of an enzymatic product, that is, the presence of the target molecule, can be confirmed using a fluorescent reporter in a short time. Accordingly, fL-chamber arrays allow rapid and accurate digital detection of target molecules.

In general, an expensive fluorescence microscope with a high magnification and high numerical aperture (NA) objective lens is used to detect fluorescence signals from fL-chambers. Since the trade-off between magnification and imaging area, using a high-magnification objective lens inevitably results in a smaller imaging area and fewer chambers that can be imaged simultaneously. In addition, the number of chambers to be analyzed correlates with the detection sensitivity in digital bioanalysis<sup>1</sup>; therefore, many images must be acquired by moving the array under a fluorescence microscope, considerably increasing the image acquisition time.

Recently, various imaging systems have been developed to immediately acquire a wide-field fluorescence image for the analysis of cells and large droplets (pico–nanoliter)<sup>12–14</sup>. Although they enable wide-field fluorescence imaging without a microscope, there are certain drawbacks in terms of the sensitivity, spatial resolution, or cost of the imaging sensor. Therefore, there is no inexpensive imaging system that can acquire an entire fluorescence image of a fL-chamber array at once with high sensitivity and throughput.

In this study, we developed a compact and inexpensive wide-field imaging system called COWFISH (Compact Wide-field Femtoliter-chamber Imaging System for High-speed digital bioanalysis) that can acquire an entire fluorescence image of sub-million fL-chambers at once with a spatial resolution of ~ 3 μm. Using COWFISH, we aimed to detect the viral RNA of SARS-CoV-2 using CRISPR-Cas13a<sup>15–17</sup> and further validate COVID-19 diagnosis using clinical specimens.

<sup>a</sup> Cluster for Pioneering Research, RIKEN, Japan.

<sup>b</sup> Department of Molecular Virology, Tokyo Medical and Dental University, Japan.

<sup>c</sup> Institute for Life and Medical Sciences, Kyoto University, Japan.

<sup>d</sup> Department of Chemistry and Biotechnology, Graduate School of Engineering, The University of Tokyo, Japan.

<sup>e</sup> RCAST, The University of Tokyo, Japan.

\*Corresponding author. E-mail: rikiya.watanabe@riken.jp

†Electronic Supplementary Information (ESI) available: figures S1–S2; tables S1–S2.

‡These authors contributed equally to this work.

## Experimental

### Configuration of COWFISH

COWFISH was constructed using a digital single-lens reflection (DSLR) camera (D7500, Nikon) and a low-distortion 2× telecentric lens (LSTL20H-F, Myutron) (Fig. 1). The DSLR camera has a 23.5 mm × 15.7 mm front-illuminated commercial complementary metal-oxide semiconductor (CMOS) sensor with a sensor pixel pitch of 4.2 μm/pixel. A telecentric lens with a field number (FN) of φ44 mm and NA of 0.12 was mounted directly on the DSLR camera via F-mount. To observe horizontally placed samples from below, the optical path was bent at a right angle by a mirror placed at 45° under the sample. A sample holder was mounted on a single-axis manual stage (XCRS40, MISUMI) to manually adjust the distance between the sample and lens and the focus position of the image. It was also mounted on a two-axis manual stage (XYCRSC40-A, MISUMI) using a right-angled bracket to move the sample horizontally manually.

Two LED light sources (M470L5 and M625L4, Thorlabs) with center wavelengths of 470 nm and 625 nm were installed for fluorescence excitation. Light from these LED units was collimated with condenser lenses (φ1",  $f = 16$  mm, ACL25416U-A, Thorlabs) and filtered using a single-band excitation filter for 470 nm (φ25 mm, MF475-35, Thorlabs) or for 625 nm (φ25 mm, ZET635/20x, Chroma). An excitation filter was attached to the LED mount head using a lens tube, and a condenser lens was placed between them. These LED units were placed under the sample holder at an angle of ~45° and a distance of ~10 cm to illuminate an area with a φ of ~2.5 cm. A 5 V analog signal output via a DAQ board (NI USB-6001, National Instruments) was used to control the LEDs from the computer. The light intensity at the sample plane was 1.9 mW/mm<sup>2</sup> for 470 nm and 1.7 mW/mm<sup>2</sup> for 625 nm. For fluorescence imaging, a quad-band pass emission filter (89402m, Chroma) was inserted before the mirror. The camera, lens, stage, and LEDs were fixed on a 35 cm × 45 cm breadboard using the DIY components provided by Thorlabs. The entire optics was covered with black aluminum frames to cover the light during fluorescence imaging.

### Fabrication of fL-chamber array

A fluoropolymer fL-chamber array was fabricated on a glass substrate using a combination of photolithographic techniques and dry etching, as previously reported<sup>7</sup>. A 32 mm × 24 mm cover glass (No. 1, Matsunami) was washed with water, immersed in 8 M KOH solution, sonicated for 1.5 h, and then left to soak overnight. The cover glass was then rinsed with running water for 10 min, sonicated with pure water for 10 min, and dried using an air blow gun. The cover glass was spin-coated with perfluoropolymer (9% CYTOP, AGC) at 1,000 rpm for 30 s and baked at 80°C for 10 min and 180°C for 1 h. A positive photoresist (AZ P4620, AZ Electronic Materials) was spin-coated onto the CYTOP-coated cover glass at 7,500 rpm for 30 s and baked at 100°C for 5 min. The photoresist on the CYTOP-coated cover glass was rehydrated at 60% humidity and 25°C for at least 5 min. The cover glass coated with the photoresist and CYTOP was irradiated with UV light using a mask aligner

(LA610dt, Nanometric Technology) fitted with a chrome photomask containing holes with a diameter of 1.8 μm arranged in a triangular lattice at 8-μm intervals. The cover glass was then immersed in a developer (AZ 300 MIF Developer, AZ Electronic Materials) for 1.5 min, rinsed with an unused developer, washed with pure water, and dried with an air blow gun. The CYTOP that was not covered with photoresist was removed by dry etching with O<sub>2</sub> plasma (RIE-10NR, Samco). Finally, the remaining photoresist was removed via sonication in acetone for 10 min, rinsed with 2-propanol, and washed with pure water. To fabricate a ring-shaped enclosure with a 7 mm diameter on the chamber array, UV-curable acrylic resin (5X649H, CHEMITECH) and a dispensing robot (SHOTmini, Musashi Engineering) were used. The fabricated fL-chamber array was observed using a laser microscope (VK-X1100, Keyence). The volume of a single chamber was 12.9 fL, with a diameter and depth of 3.2 ± 0.2 and 1.6 ± 0.1 μm (mean ± SD), respectively.

### Preparation of Cas13a

For the expression of LtrCas13a<sup>18</sup>, *Escherichia coli* Rosetta 2 (DE3) was transformed with the pET-LtrCas13a plasmid, and the cells were cultured in a 2.5-L LB medium containing kanamycin. When the OD<sub>600</sub> values reached 0.6–1.0, the cells were cooled on ice for 10 min and further cultured at 20°C for 20 h with 0.1 mM IPTG. Bacterial cells were collected by centrifugation, suspended in 40 mL of buffer A (20 mM Tris-HCl [pH 8.0], 1 M NaCl, 20 mM imidazole, 3 mM β-mercaptoethanol, and 1 mM phenylmethylsulfonyl fluoride), and lysed via sonication (Q500, QSONICA). After centrifugation at 15,000 rpm for 20 min, the supernatant was incubated with Ni-NTA agarose (Qiagen) at 4°C for 1 h. The mixture was then transferred to an Econo column (Bio-Rad). The resin was washed with buffer B (20 mM Tris-HCl [pH 8.0], 0.3 M NaCl, 20 mM imidazole, and 3 mM β-mercaptoethanol), and the protein was eluted with buffer C (20 mM Tris-HCl [pH 8.0], 0.3 M NaCl, 300 mM imidazole, and 3 mM β-mercaptoethanol). The protein was then loaded onto a HiTrap SP HP column (Cytiva) equilibrated with buffer D (50 mM HEPES-KOH [pH 7.5], 0.3 M NaCl, and 0.5 mM TCEP). The protein was eluted using a linear gradient from 0.3 to 2.0 M NaCl over seven column volumes. It was further purified through size exclusion chromatography (Enrich SEC 650, Bio-Rad) with buffer E (50 mM HEPES-KOH [pH 7.5], 0.5 M NaCl, and 0.5 mM TCEP).

### Preparation of crRNA, FQ-reporter, and SARS-CoV-2 viral RNA

Chemical synthesis crRNA targeting the N-gene of SARS-CoV-2 (GGAUUUAGAGUACCCCAAAAUGAAGGGGACUAAAACUUGGC AAUGUUGUUCUUGAGGAAGUUGUAGC) was purchased from GeneDesign. The FQ-reporter (FAM/rUrUrUrU/3IABkFQ) and FAM-polyU (FAM/rUrUrUrU) were purchased from IDT. SARS-CoV-2 viral RNA was prepared as follows: SARS-CoV-2/Hu/DP/Kng/19-027 (Wuhan lineage) was propagated in VeroE6/TMPRSS2 cells (JCRB 1819), which were cultured in Dulbecco's modified Eagle's medium (DMEM, Sigma-Aldrich) containing 5% fetal calf serum (FCS) and 1% penicillin/streptomycin at 37°C under 5% CO<sub>2</sub>. Viral supernatants were collected 2 days after infection, and the viral

RNA was purified using an RNeasy kit (Qiagen). The concentration of the viral RNA was determined from the A260 value measured using a Nano Drop spectrophotometer.

#### SARS-CoV-2 patient samples

Nasopharyngeal swab samples were collected from 10 SARS-CoV-2 patients and 10 healthy persons at the Tokyo Medical and Dental University Hospital. RNA was extracted from the samples using the QIAamp Viral RNA Mini Kit (Qiagen) according to the manufacturer's protocol. The RNA was eluted in nuclease-free water. RT-qPCR was performed using the extracted RNA with QuantStudio 3 (Thermo Fisher Scientific) and Ampdirect™ 2019-nCoV Detection Kit with a primer set targeting the N-gene region of SARS-CoV-2 RNA (SHIMADZU). The SARS-CoV-2 viral RNA purified from VeroE6/TMORSS2 cells (Wuhan strain) was used as a reference to obtain a calibration curve of RT-qPCR Ct values and the copy number of SARS-CoV-2 viral RNA. Whole viral genome sequences (WGS) of SARS-CoV-2 from patients were analyzed using MiSeq (Illumina). This research was approved by the Tokyo Medical and Dental University (approval ID number: M2020-004), and informed consent was obtained from all participants.

#### SATORI assay

The assay solution for SATORI (solution A) for a single assay was prepared as follows: To prepare Cas13a-crRNA complexes, a mixture of 0.7  $\mu\text{L}$  of Cas13a (20  $\mu\text{M}$ ), 1.4  $\mu\text{L}$  of crRNA, and 2.6  $\mu\text{L}$  of buffer F (20 mM HEPES-KOH [pH 6.8], 60 mM NaCl, 6 mM  $\text{MgCl}_2$ , and 50  $\mu\text{M}$  Triton X-100) was incubated at 37°C for 10 min. Next, 4.7  $\mu\text{L}$  of Cas13a-crRNA solution was mixed with 18.7  $\mu\text{L}$  of buffer G (20 mM HEPES-KOH [pH 7.5], 100 mM NaCl, 10 mM  $\text{MgCl}_2$ , 50  $\mu\text{M}$  Triton X-100, 15  $\mu\text{M}$  FQ-reporter [IDT], and 75  $\mu\text{M}$  Alexa Fluor™ 647 C2 maleimide [Thermo Scientific]), and stored at  $-80^\circ\text{C}$  until use.

Before starting the SATORI assay, frozen solution A was thawed at 25°C. Then 20  $\mu\text{L}$  of solution A was mixed with 100  $\mu\text{L}$  of target RNA solution. After 1 min of incubation, 105  $\mu\text{L}$  of the mixture was dropped onto an fL-chamber array. Of the 105- $\mu\text{L}$  solution on the array, 95  $\mu\text{L}$  was removed, and 50  $\mu\text{L}$  of Fomblin oil (Y LVAC 25/6, Solvay) was added to seal the microchamber. The excess solution A and Fomblin oil left on the array were removed. After 3 min of incubation, fluorescence images were acquired using COWFISH or confocal microscope with a 20 $\times$  objective lens (NA = 0.75), 488 nm and 640 nm lasers, and a motorized 2-axis scanning stage (A1HD25, Nikon). For COWFISH, fluorescence images were acquired for 20 s (10 s for ex. 470 nm, 10 s for ex. 625 nm). For confocal microscopy, fluorescence tiling images with 488 nm and 640 nm lasers were acquired for approximately 200 s with 64-stage scanning.

#### Image acquisition and processing of COWFISH

The considerable depth of field of the telecentric lens (0.12 mm) makes it easier to adjust and hold the sample in focus with COWFISH than with confocal microscopy. However, the focus position for red imaging was 150  $\mu\text{m}$  from that of the green imaging due to a chromatic aberration. The z-position of the

sample was moved 150  $\mu\text{m}$  to acquire a red image after acquiring a green image. Fluorescence and bright-field images were acquired in NEF (Nikon RAW) format using an open-source software (digiCamControl) with ISO 100; NEF images were then converted to TIFF format using a software (NX Studio, Nikon).

#### Evaluation of pixel size and spatial resolution of COWFISH

Bright-field images of a stage micrometer (OBM1/100SQ, Olympus), which has lines at 10- $\mu\text{m}$  intervals, were acquired at the center and four corners of the field of view (FOV). By dividing the distance of 200  $\mu\text{m}$  by the number of pixels on the image, the pixel sizes were calculated for both the x- and y-axis at five positions.

The fluorescent beads were prepared by mixing 10 mg/mL magnetic beads ( $\phi$ 1  $\mu\text{m}$ , MyOneT1, Invitrogen) with ATTO 488 biotin and ATTO 647N biotin (ATTO-TEC), incubating at 25°C for 10 min, washing with buffer G three times, and adjusting the concentration to 1  $\mu\text{g}/\text{mL}$  with buffer G. The fluorescent beads were then immobilized on the surface of a 32 mm  $\times$  24 mm cover glass (No. 1, Matsunami) via non-specific interaction. The fluorescence images were acquired at the center and four corners of the FOV via sequential illumination at 470 nm for green fluorescence and 625 nm for red fluorescence.

#### Data analysis for SATORI assay

The 16-bit Tagged Image File Format (TIFF) images obtained by COWFISH were analyzed using ImageJ software as follows: Fluorescence images were processed by removing the background signal with ImageJ's Subtract Background command (parameter: 50-pixel rolling ball radius), followed by ImageJ's Scale command (parameters: a scale factor of 2.0 for both the x- and y-axis, and bilinear interpolation) to improve Region of Interest (ROI) recognition of adjacent chambers in the subsequent analysis. The green image was then binarized using an intensity of 12,000 as a threshold. To determine the positive chambers and obtain ROI information, the binarized images were processed using ImageJ's Analyze Particles command (parameters: size 7–50  $\mu\text{m}^2$ , circularity 0.8–1.0). Under this criterion, some dust on the substrate can be detected, causing false positives. Since most dust shows a strong fluorescence signal in both green and red images, the fluorescence intensity of the red image in the ROI was used to suppress the counting of false-positive chambers. The ratio of the fluorescence intensity in the green and red images (red/green ratio) was calculated, and the ROIs with a red/green ratio greater than 0.1 were excluded as false-positive chambers.

The 10-bit TIFF images (red and green) obtained by confocal microscopy were analyzed using NIS-Elements software (Nikon), as follows: The green images were processed using the NIS-Elements Object Count command (parameters: diameter: 3–8  $\mu\text{m}$ , circularity: 0.8–1.0, threshold: 2,000) to determine the positive chambers and obtain their ROI information. In the same way as COWFISH, the fluorescence intensity of the red image in the ROI was used to suppress the counting of false-positive chambers. The ROIs with a red/green ratio greater than 0.5 were excluded as false-positive chambers.

The analytical limit of detection (LoD) was defined as follows: the number of positive chambers obtained with different concentrations of the target RNA (tgRNA) was fitted to a linear curve. The mean + 3 SD value for the number of positive chambers obtained without tgRNA was determined, and the crossing point of the linear curve and the mean + 3 SD value were then determined. The concentration corresponding to the crossing point was defined as the LoD value.

## Results & discussion

### Development of COWFISH

To expand the versatility of digital bioanalysis, we developed a compact and inexpensive wide-field imaging system (COWFISH) that can simultaneously acquire an entire fluorescence image of sub-million fL-chambers (Fig. 1). COWFISH consists of a commercial DSLR camera, telecentric lens, and LED illumination system, and is compact, measuring 35 cm (w) × 45 cm (d) × 30 cm (h) (Fig. 1C). Low-distortion telecentric lenses are widely used for wide-field high-resolution imaging such as machine vision applications<sup>19</sup>. The image pixel pitch of COWFISH was 2.1 μm/pixel, regardless of the position in FOV, determined by bright-field observation of a micrometer; from the size of the CMOS sensor (5568 pixel × 3712 pixel), FOV was 11.8 (x) × 7.9 mm (y) (Fig. S1, Table S1). These values coincide with those calculated theoretically from the magnification of the telecentric lens. The FOV of COWFISH is large enough to observe a single well (ϕ7 mm) in a 96-well plate assay or sub-million fL-chambers (ϕ~3 μm) for digital bioanalysis.

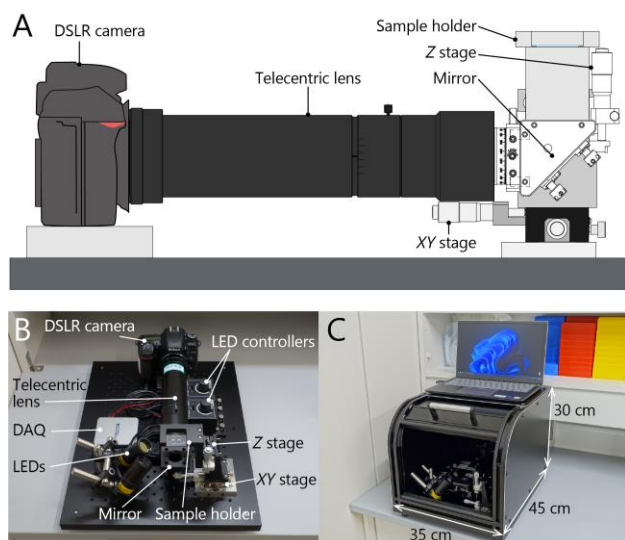


**Fig. 1** COWFISH: Compact wide-field fL-chamber imaging system. (A) Illustration (side view), (B) photograph (top view), and (C) (complete view) of COWFISH: 35 cm (w) × 45 cm (d) × 30 cm (h).

To assess spatial resolution, fluorescence images of magnetic beads of ϕ1 μm labeled with ATTO 488 and ATTO 647N were acquired using COWFISH. A total of 250 beads were analyzed at five positions (center and four corners on FOV) to determine the x- and y-intensity profiles, which were then fitted with a

Gaussian function to calculate the value of the full width at half maximum (FWHM), a parameter of spatial resolution (Fig. 2).

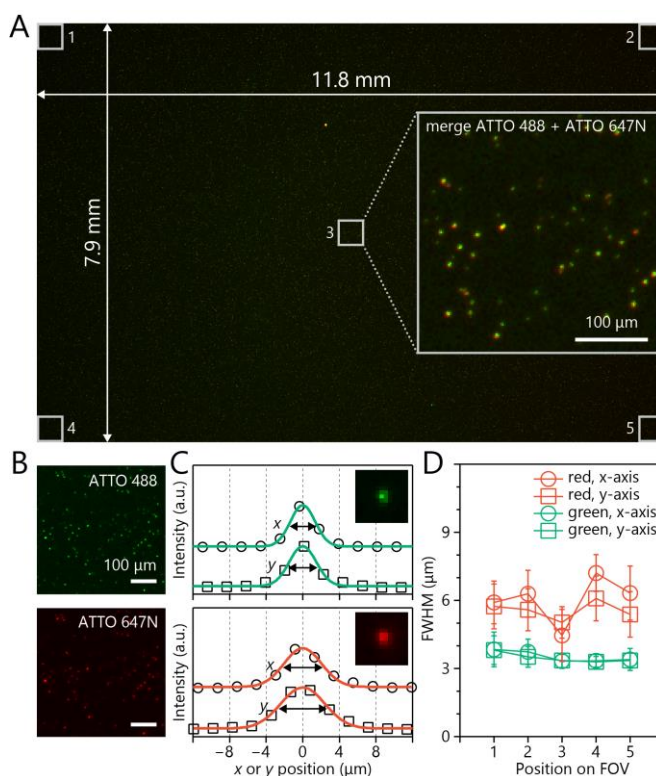


**Fig. 2** Two-color fluorescence imaging with COWFISH. (A) Fluorescence image of magnetic beads (ϕ1 μm) labeled with ATTO 488 (green) and ATTO 647N (red). (B) Enlarged view of position 3 in (A). (C) Representative of the derived intensity profile. Inset is the representative fluorescence image. (D) FWHM calculated from (C) (n = 5 technical replicates).

The FWHM of the green (wavelength ~520 nm) and red (wavelength ~690 nm) fluorescence images of the beads at the center of FOV was calculated as  $3.3 \pm 0.3$  and  $3.4 \pm 0.3$  μm for the green channel and  $4.4 \pm 1.1$  μm and  $5.0 \pm 0.7$  μm for the red channel (mean ± SD for x- and y-axis, respectively). The ratio of detected wavelengths ( $520/690 = 0.75$ ) is almost the same as the ratio of FWHM of the green and red channels ( $3.4/4.7 = 0.72$ ), which is in agreement with the theory that spatial resolution decreases linearly with wavelength.

The FWHM for the green channel was almost constant regardless of the image position and is in good agreement with the theoretical values provided by the lens manufacturer (2.9 μm at 550 nm) (Fig. 2, Table S1); however, the FWHM for the red channel was dependent on the image position, i.e., 4.7 μm at the center and 6.0 μm at the corner of FOV (as an average of four corners along x- and y-axis) (Fig. 2, Table S1). The increase in the FWHM in the red channel at the corner of the image can be attributed to aberrations of the telecentric lens. Although there is room for further improvement in the spatial resolution at the corners of FOV in the red channel, COWFISH can be used to observe the fL-chamber arrays with a chamber pitch of 8 μm, as used in this study.

### Fluorescence imaging of fL-chamber array

To confirm the linearity of the fluorescence intensity in COWFISH, we performed fluorescence imaging using fL-chamber arrays containing various concentrations of

fluorescent dye (FAM-polyU) (Fig. 3). Under an exposure time of 10 s, the fluorescence intensity in the chambers proportionally increased with the concentration of FAM-polyU in the range of 1  $\mu\text{M}$  to 10  $\mu\text{M}$  (Fig. 3B), indicating that COWFISH, that is, a commercial DSLR camera, can be applied for high-speed and quantitative digital bioanalysis using fL-chamber arrays. The fluorescence decay was only 4% after exposure for 10 s (Fig. S2), indicating the applicability of time-lapse imaging in digital bioanalysis.

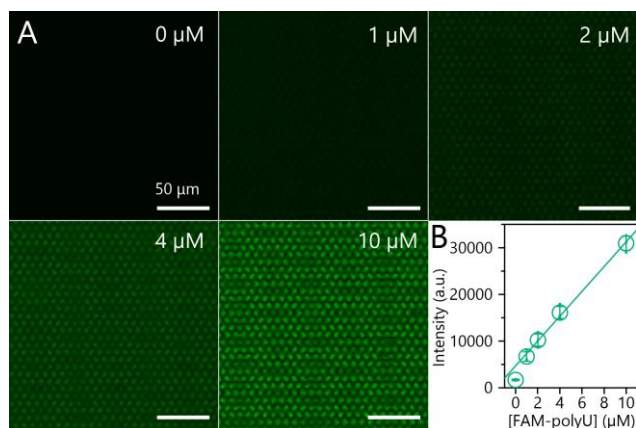


**Fig. 3** Fluorescence imaging of fL-chamber arrays. (A) Representative fluorescence image of fL-chambers at each concentration of FAM-polyU (green). (B) Fluorescence intensity in the fL-chamber is plotted against the concentration of FAM-polyU. The solid line indicates the linear regression. ( $n = 3$  technical replicates)

#### Digital bioanalysis (digital viral RNA detection)

As a proof-of-concept for digital bioanalysis, we examined the feasibility of COWFISH for digital viral RNA detection using CRISPR-Cas13a (SATORI)<sup>7</sup> and compared it with the conventional method using confocal microscopy (Fig. 4). Considering the recent global pandemic, viral RNA derived from SARS-CoV-2 was selected as the target for the SATORI assay<sup>20</sup>. In SATORI assay, a mixture of SARS-CoV-2 viral RNA (target RNA (tgRNA)), LtrCas13a in complex with crRNA (targeting N-gene of SARS-CoV-2)<sup>8</sup>, and fluorescent reporters (FAM-based: FQ-reporter) was dropped on the arrays and confined into the fL-chambers by dropping an oil. After incubation for a few minutes, the fL-chambers which include Cas13a-crRNA-tgRNA complexes represent fluorescence signal due to cleavage of FQ reporters, and were counted quantitatively as positive chambers from obtained fluorescence images. Notably, SATORI assay uses a fL-chamber array with  $\phi 7$  mm enclosure, the same size as single wells in 96-well-plate, containing  $\sim 650,000$  of fL-chambers.

Using COWFISH, the entire fL-chamber arrays can be acquired as a single image in 20 s (10 s for ex. 470 nm, 10 s for ex. 625 nm), whereas the confocal microscope with a 20 $\times$  objective lens requires dividing the same image area into  $\sim 64$  FOV and took approximately 200 s for image acquisition. Over a wide range of SARS-CoV-2 viral RNA concentrations ( $\sim 500$  aM–300 fM), the number of positive chambers determined by COWFISH analysis increased linearly, as observed via confocal microscopy (Fig. 5), indicating that COWFISH can be used for tgRNA quantification. The LoD value obtained using COWFISH was 480 aM, almost the

same as that obtained using confocal microscopy (Fig. 5B). Because the LoD is primarily determined by the trapping efficiency of the target molecule inside the chamber and the amount of background signal, i.e., the LoD is equivalent under the same imaging sensitivity,<sup>21</sup> it is highly probable that COWFISH has imaging sensitivity comparable to confocal microscopy for the SATORI assay. These results indicate that COWFISH can be used instead of confocal microscopy for digital bioanalysis with fL-chamber arrays.

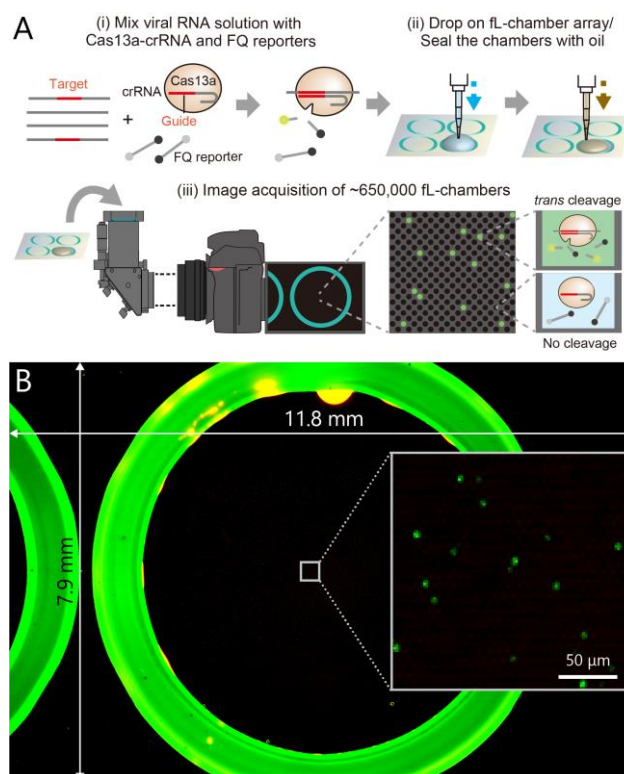


**Fig. 4** Digital viral RNA detection using CRISPR-Cas13a (SATORI). (A) Schematic illustration of SATORI assay. Upon viral RNA binding, the Cas13a-crRNA complex cleaves FQ reporters, resulting in increased fluorescence in the fL-chamber. (B) Single fluorescence image acquired by COWFISH. The green circle represents the enclosure of  $\phi 7$  mm, which contains  $\sim 650,000$  fL-chambers. Inset is the zoom-up.

#### Clinical validation

We examined whether COWFISH can be used to diagnose SARS-CoV-2 infection based on the SATORI assay (Fig. 6). Using the same crRNA, we evaluated the number of positive chambers from 10 nasopharyngeal swab-derived RNA samples from SARS-CoV-2 patients with Ct values of 19–28 (2 WT, 2 alpha, 2 Japan, 2 delta, and 2 omicron variants) and 10 RNA samples from healthy persons. The number of positive chambers for the patient samples correlated well with their copy numbers (Ct values) determined using RT-qPCR, with a correlation coefficient of 0.90 (Fig. 6C). Accordingly, we could distinguish between SARS-CoV-2 positive and negative samples with an accuracy of 95% (number of trials using SATORI matched to RT-qPCR/total number of trials of SATORI) and a positive precision rate of 100% (number of positive trials using SATORI/number of positive trials using RT-qPCR) by using a positive threshold

(number of positive chambers is  $\geq 10$ ), as previously employed in SATORI<sup>8</sup> (Fig. 6A, B). These results demonstrate the potential of COWFISH for rapid and accurate clinical disease diagnosis, including COVID-19.

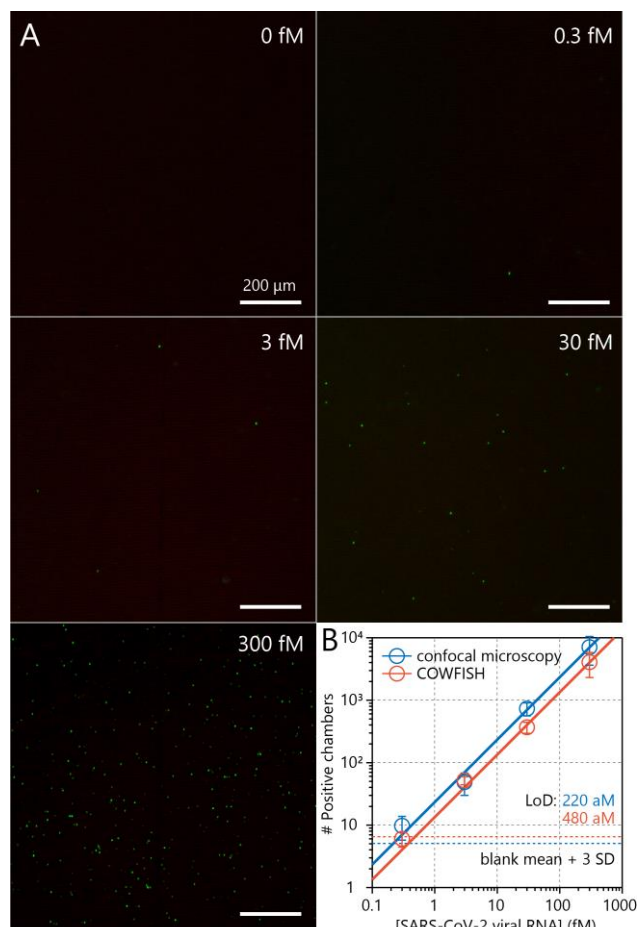


**Fig. 5** Digital counting of viral RNA of SARS-CoV-2. (A) Representative fluorescence image at each concentration of SARS-CoV-2 viral RNA. (B) The number of positive chambers obtained with COWFISH (red) or confocal microscopy (blue). The solid lines indicate linear regressions. The values of the blank mean + 3 SD are indicated by dotted lines ( $n = 3$  technical replicates).

## Conclusions

We developed a device representing a new class of wide-field imaging systems called COWFISH that can acquire fluorescence images of sub-million fL-chambers with a spatial resolution of  $\sim 3 \mu\text{m}$ . Digital bioanalysis using COWFISH demonstrated a detection sensitivity equivalent to that of confocal microscopy, along with a reduction in the total imaging time by a factor of 10. COWFISH costs approximately US\$8,700 (Table S2), which is approximately 1/30th that of confocal microscopy. Together, these advantages strongly support the application of COWFISH in high-speed and low-cost digital bioanalysis.

COWFISH also demonstrated digital detection of viral RNA of SARS-CoV-2 with a detection sensitivity of 480 aM and further validated COVID-19 diagnosis using clinical specimens (discrimination of SARS-CoV-2 positive and negative samples with 95% accuracy). In addition, COWFISH is constructed using

simple and inexpensive components, resulting in a compact size of 35 cm (w)  $\times$  45 cm (d)  $\times$  30 cm (h). Thus, we envision that COWFISH will be implemented in town clinics and airport quarantine stations as a versatile platform for high-speed, high-accuracy, and low-cost diagnosis of various viral infections, including COVID-19<sup>22</sup>.

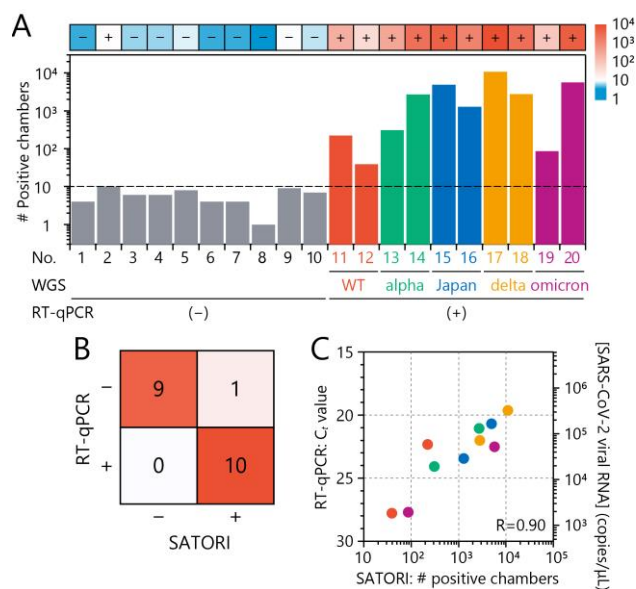


**Fig. 6** Clinical validation. (A) Detection of SARS-CoV-2 in clinical specimens. The dashed line indicates the positive threshold (number of positive chambers  $\geq 10$ ). (B) Comparison of SATORI-COWFISH and RT-qPCR results in SARS-CoV-2 detection. (C) Comparison of SATORI-COWFISH and RT-qPCR for quantification of the SARS-CoV-2 viral RNA copy number.

## Author Contributions

T.I. and J.A. contributed equally to the work; T.I., J.A., and R.W. designed the experiments; H.S., A.M., M.Y., K.M., and M.M. performed sample preparation; T.I., J.A., and R.W. developed COWFISH; T.I. performed the SATORI assays; H.T., T.N., H.N., and R.W. supervised the study; T.I., J.A., H.S., and R.W. wrote the manuscript.

## Conflicts of interest

There are no conflicts to declare.

## Acknowledgements

We thank all members of the Watanabe, Nishimasu, Noda, and Takeuchi laboratories for their constructive discussions, as well as the Advanced Manufacturing Support Team at RIKEN for technical assistance. This work was supported by JST CREST (JPMJCR19H5), AMED (20he0622032h0001, 20fk0108529h0001, and 21fk0108423h0001), and the Mitsubishi Foundation Grant for Academic Research on Infectious Diseases, including COVID-19 to H.N. and R.W.; JSPS Grant-in-Aid for Scientific Research A (21H04645) to H.T., T.N., H.N., and R.W.; and JSPS Grant-in-Aid for Transformative

Research Areas A (20H05931) and AMED (JP22he0422018) to R.W.; JST CREST (JPMJCR20HA) and JSPS Core-to-Core program A, to T.N.

## Notes and references

- H. Noji, Y. Minagawa and H. Ueno, *Lab Chip*, 2022, DOI: 10.1039/d2lc00223j.
- L. Cohen and D. R. Walt, *Annu Rev Anal Chem (Palo Alto Calif)*, 2017, **10**, 345-363.
- T. Gilboa, A. F. Ogata, C. B. Reilly and D. R. Walt, *Biophys J*, 2022, **121**, 2027-2034.
- Y. Zhang, Y. Minagawa, H. Kizoe, K. Miyazaki, R. Iino, H. Ueno, K. V. Tabata, Y. Shimane and H. Noji, *Sci Adv*, 2019, **5**, eaav8185.
- R. Watanabe, T. Sakuragi, H. Noji and S. Nagata, *Proc Natl Acad Sci U S A*, 2018, **115**, 3066-3071.
- R. Watanabe, N. Soga, D. Fujita, K. V. Tabata, L. Yamauchi, S. Hyeon Kim, D. Asanuma, M. Kamiya, Y. Urano, H. Suga and H. Noji, *Nat Commun*, 2014, **5**, 4519.
- H. Shinoda, Y. Taguchi, R. Nakagawa, A. Makino, S. Okazaki, M. Nakano, Y. Muramoto, C. Takahashi, I. Takahashi, J. Ando, T. Noda, O. Nureki, H. Nishimasu and R. Watanabe, *Commun Biol*, 2021, **4**, 476.
- H. Shinoda, T. Iida, A. Makino, M. Yoshimura, J. Ishikawa, J. Ando, K. Murai, K. Sugiyama, Y. Muramoto, M. Nakano, K. Kiga, L. Cui, O. Nureki, H. Takeuchi, T. Noda, H. Nishimasu and R. Watanabe, *Commun Biol*, 2022, **5**, 473.
- S. Sakamoto, T. Komatsu, R. Watanabe, Y. Zhang, T. Inoue, M. Kawaguchi, H. Nakagawa, T. Ueno, T. Okusaka, K. Honda, H. Noji and Y. Urano, *Sci Adv*, 2020, **6**, eaay0888.
- D. M. Rissin, C. W. Kan, T. G. Campbell, S. C. Howes, D. R. Fournier, L. Song, T. Piech, P. P. Patel, L. Chang, A. J. Rivnak, E. P. Ferrell, J. D. Randall, G. K. Provuncher, D. R. Walt and D. C. Duffy, *Nat Biotechnol*, 2010, **28**, 595-599.
- K. Kulenkampff, A. M. Wolf Perez, P. Sormanni, J. Habchi and M. Vendruscolo, *Nat Rev Chem*, 2021, **5**, 277-294.
- T. Ichimura, T. Kakizuka, K. Horikawa, K. Seiriki, A. Kasai, H. Hashimoto, K. Fujita, T. M. Watanabe and T. Nagai, *Sci Rep*, 2021, **11**, 16539.
- A. C. Hatch, J. S. Fisher, A. R. Tovar, A. T. Hsieh, R. Lin, S. L. Pentoney, D. L. Yang and A. P. Lee, *Lab Chip*, 2011, **11**, 3838-3845.
- Z. Yan, H. Zhang, X. Wang, M. Ganova, T. Lednický, H. Zhu, X. Liu, M. Korabecna, H. Chang and P. Neuzil, *Lab Chip*, 2022, **22**, 1333-1343.
- J. S. Gootenberg, O. O. Abudayyeh, J. W. Lee, P. Essletzbichler, A. J. Dy, J. Joung, V. Verdine, N. Donghia, N. M. Daringer, C. A. Freije, C. Myhrvold, R. P. Bhattacharyya, J. Livny, A. Regev, E. V. Koonin, D. T. Hung, P. C. Sabeti, J. J. Collins and F. Zhang, *Science*, 2017, **356**, 438-442.
- A. East-Seletsky, M. R. O'Connell, D. Burstein, G. J. Knott and J. A. Doudna, *Mol Cell*, 2017, **66**, 373-383 e373.
- Y. Li, S. Li, J. Wang and G. Liu, *Trends Biotechnol*, 2019, **37**, 730-743.
- S. Watanabe, B. Cui, K. Kiga, Y. Aiba, X. E. Tan, Y. Sato'o, M. Kawauchi, T. Boonsiri, K. Thititanapakorn, Y. Taki, F. Y. Li, A. H. Azam, Y. Nakada, T. Sasahara and L. Cui, *Front Microbiol*, 2019, **10**, 2838.
- J. Beyerer, F. Puente Leon and C. Frese, *Machine Vision : Automated Visual Inspection: Theory, Practice and Applications*. Berlin: Springer, 2016.
- E. Dong, H. Du and L. Gardner, *Lancet Infect Dis*, 2020, **20**, 533-534.
- S. H. Kim, S. Iwai, S. Araki, S. Sakakihara, R. Iino and H. Noji, *Lab Chip*, 2012, **12**, 4986-4991.
- D. B. Larremore, B. Wilder, E. Lester, S. Shehata, J. M. Burke, J. A. Hay, M. Tambe, M. J. Mina and R. Parker, *Sci Adv*, 2021, **7**.